



WILEY

ORIGINAL RESEARCH REPORT

An effective dual-factor modified 3D-printed PCL scaffold for bone defect repair

Yan Li^{1,2,3} | Qian Li^{2,3} | Hongming Li⁴ | Xiao Xu^{1,2} | Xiaoming Fu^{1,2} | Jijia Pan² | Hui Wang⁵ | Jerry Ying Hsi Fuh⁵ | Yanjie Bai⁶ | Shicheng Wei^{1,2,3}

¹Department of Oral and Maxillofacial Surgery, Central Laboratory, School and Hospital of Stomatology, Peking University, Beijing, China

²Laboratory of Biomaterials and Regenerative Medicine, Academy for Advanced Interdisciplinary Studies, Peking University, Beijing, China

³Key Laboratory of Military Stomatology, Hospital of Stomatology, the Fourth Military Medical University, Xi An, China

⁴College of Pharmacy, Jiangxi Normal University of Science and Technology, Nanchang, China

⁵Suzhou Research Institute, National University of Singapore, Suzhou, China

⁶Department of Stomatology, Peking University Third Hospital, Peking University, Beijing, China

Correspondence

Yanjie Bai, Department of Stomatology, Peking University Third Hospital, Peking University, Beijing 100191, China.

Email: yanjiebai@126.com

Shicheng Wei, Department of Oral and Maxillofacial Surgery, Central Laboratory, School and Hospital of Stomatology, Peking University, Beijing 100081, China.
Email: sc-wei@pku.edu.cn

Funding information

Open Project from State Key Laboratory of Military Stomatology, Grant/Award Number: 2016KA01; Peking University's 985 Grant; the National Natural Science Foundation of China, Grant/Award Number: 81571814

Abstract

Numerous bioactive molecules produced in cells are involved in the process of bone formation. We consider that appropriate, simultaneous application of two types of bioactive molecules would accelerate the regeneration of tissues and organs. Therefore, we combined aspirin-loaded liposomes (Asp@Lipo) and bone forming peptide-1 (BFP-1) on three dimensional-printed polycaprolactone (PCL) scaffold and determined whether this system improved bone regeneration outcomes. *in vitro* experiments indicated that Asp@Lipo/BFP-1 at a 3:7 ratio was the best option for enhancing the osteogenic efficiency of human mesenchymal stem cells (hMSCs). This was confirmed in an *in vivo* cranial defect animal model. In addition, RNA-Seq was applied for preliminary exploration of the mechanism of action of this composite scaffold system, and the results suggested that it mainly improved bone regeneration via the PI3K/AKT signaling pathway. This approach will have potential for application in bone tissue engineering and regenerative medicine.

KEYWORDS

aspirin, BFP-1, bone regeneration, drug delivery system, liposomes

1 | INTRODUCTION

Surgical repair using bone biomaterial is often required for bone defects caused by traumatic fractures, tumor resection, osteomyelitis, or osteolysis (Carson & Bostrom, 2007; Cook & Cook, 2009; Oliveira, Hage, Carrel, Lombardi, & Bernard, 2012; Schindler, Cannon, Briggs, &

Blunn, 2007). Due to the direct relationship between osteoblasts and bone formation, the ability to regulate the differentiation of osteoblasts is the main goal of bone biomaterial-based treatments at present. However, research has mostly focused on optimizing the composition, and physicochemical and mechanical properties, of such materials; the requirement for further optimization of fundamental biological principles has often been neglected. Bone defect repair is an extremely complex physiological process, which is largely mediated

Yan Li and Qian Li authors contributed equally to this work.

and regulated by the injured cells and other recruited cells (Fernandez-Tresguerres-Hernandez-Gil & Alobera-Gracia, 2006; Fernandez-Tresguerres-Hernandez-Gil, Alobera-Gracia, del-Canto-Pingarron, & Blanco-Jerez, 2006). Due to the small number of cells in defect sites caused by immune diseases, regeneration of bone defects is difficult, and self-repair is often slow and ineffective (Arboleya & Castañeda, 2013; Sambuceti et al., 2009; Smilek, Ehlers, & Nepom, 2014). The results of animal bone defect models showed that when the defect size exceeded a critical threshold, the self-repair ability was not be sufficient to restore function, such that tissue engineering-based interventions are needed (Schmitz & Hollinger, 1986).

To address the above problems, drug delivery systems could serve as an effective alternative method (Anselmo & Mitragotri, 2014; Vo, Kasper, & Mikos, 2012). Drugs can be loaded into carriers composed of suitable materials, and then released in a sustained way to facilitate the physiological response to local damage (Bajpai, Shukla, Bhanu, & Kankane, 2008; Bawa, Pillay, Choonara, & du Toit, 2009; Jain, 2008; Vo et al., 2012). Considering the complexity of the bone regeneration process, a sustained-release system comprising only one drug may not be sufficient for optimal bone remodeling. As use of multiple drugs not only promotes osteogenesis, but also regulates inflammation and angiogenesis (Arboleya & Castañeda, 2013; Dimitriou, Tsiridis, & Giannoudis, 2005; Lind & Bunger, 2001; Saran, Gemini Piperni, & Chatterjee, 2014; Trueta, 1963; Tsiridis, Upadhyay, & Giannoudis, 2007), it would be preferable to release multiple types of molecules or drugs from carriers to promote bone remodeling, in a controllable manner with respect to place and time.

In recent years, three dimensional (3D) printing technology has been widely used in various fields such as biomedicine due to its accuracy and simplicity of operation (Zadpoor & Malda, 2017). Polycaprolactone (PCL) scaffolds are often used in bone tissue engineering because of their good biocompatibility and controllable degradation. Although 3D-printed scaffolds generally have a certain mechanical support ability, the porosity of scaffolds is generally low, and the surface does not have good biological activity, which is insufficient to provide an ideal internal environment for cell proliferation and differentiation (Kawaguchi et al., 1994; Perets et al., 2003). Therefore, it is necessary to modify PCL scaffolds with molecules or drugs to improve their osteogenic ability.

Bone morphogenetic proteins (BMPs), as osteogenic growth factors, have a positive effect on bone regeneration through Smad/MAPK pathway (Beederman et al., 2013). Furthermore, while some results indicated that BMPs may facilitate bone remodeling, other studies stated that the high cost and side effects (osteolysis and even ectopic bone formation) of BMPs cannot be ignored (Oryan, Alidadi, Moshiri, & Bigham-Sadegh, 2014). Fortunately, bone-forming peptide-1 (BFP-1), which is present in the immature region of BMP-7 protein and is composed of 15 amino acids, showed higher osteogenic induction activity than BMP-7 protein, suggesting its potential for promoting osteodifferentiation of hMSCs (Kim et al., 2012).

The development of osteoimmunology has shown that the skeletal system and immune system are closely associated and share many cytokines, transcription factors, and receptors (Arron & Choi, 2000; Takayanagi, 2007). The field of osteoimmunology investigates the

relationship between the skeletal and immune systems, focusing on various interrelated cellular and molecular signaling pathways connecting the bone and immune systems to regulate these processes in inflammatory bone diseases, such as osteoporosis, rheumatoid arthritis, and osteoarthritis (Cook & Cook, 2009). Bone diseases, which lead to imbalance between the immune and bone systems, accelerate bone loss. It has been shown in various animal models that the breakdown of the inflammatory cascade at any time can effectively attenuate bone loss (Staiger, Pietak, Huadmai, & Dias, 2006; Wang et al., 2012). Aspirin is a nonsteroidal anti-inflammatory drug (NSAID) that has also been shown to inhibit osteoclast formation and improve bone formation (Bessa et al., 2010). Liposomes are formed by lipids self-assembly with a bilayer structure. They can be a nanosized, biodegradable, low toxicity, and less immunogenic drug delivery vehicle to control drug loading and release. A previous study demonstrated the potential applicability of PCL scaffolds based on an aspirin liposome sustained-release system for promoting bone formation (Li et al., 2019).

Our preliminary experimental results raised questions regarding whether the combination of aspirin-loaded liposomes (Asp@Lipo) and BFP-1 could have better therapeutic efficacy in the complex bone remodeling process (Li et al., 2019). Therefore, we constructed a composite scaffold system based on PCL substrate for accelerated bone remodeling by grafting a drug sustained-release system (aspirin-loaded liposomes) and growth factor (BFP-1). We studied its effects with respect to the osteogenic differentiation of hMSCs and bone regeneration in vivo (Figure 1). Transcriptome sequencing technology was used to study the mechanism of bone regeneration and determine the optimal conditions for bone integration, according to the balance between the generation of osteoblasts and osteoclasts. Our results suggest that 3D-printed PCL scaffold decorated Asp@Lipo and BFP-1 has significant osteogenic ability, which may promote the development and future clinical applications of bone immunological biomaterials.

2 | MATERIALS AND METHODS

2.1 | Materials

Aspirin and dopamine hydrochloride (DA) were obtained from Sigma-Aldrich (St. Louis, MO). BFP-1 (>98%; sequence, GQGFSYPYKAVFSTQ) was purchased from ChinaPeptides Co., Ltd. (Shanghai, China). PCL scaffolds were provided by the National University of Singapore Suzhou Research Institute. 2-(*N*-morpholino) ethanesulfonic acid (MES), *N*-hydroxysuccinimide (NHS), and 1-(3-dimethylaminopropyl)-3-ethylcarbodiimide (EDC) were purchased from Aladdin (Shanghai, China). Tris[hydroxymethyl]-aminomethane (Tris-HCl) was purchased from Sinopharm Chemical Reagent Co. Ltd. (Beijing, China). α -phosphatidylethanolamine-*N*-(lissamine rhodamine B sulfonyl) (PE-Rho) was purchased from Avanti Polar Lipids (Alabaster, AL). Cholesterol was provided by Sigma-Aldrich. 1,2-distearoyl-sn-glycero-3-phosphoethanolamine-*N*-amino (poly[ethylene glycol])-2000 (DSPE-PEG-NH₂) was purchased from Ruixi Biological Technology Co., Ltd. (Shaanxi, China). 1,2-dipalmitoyl-sn-glycero-3-phosphocholine

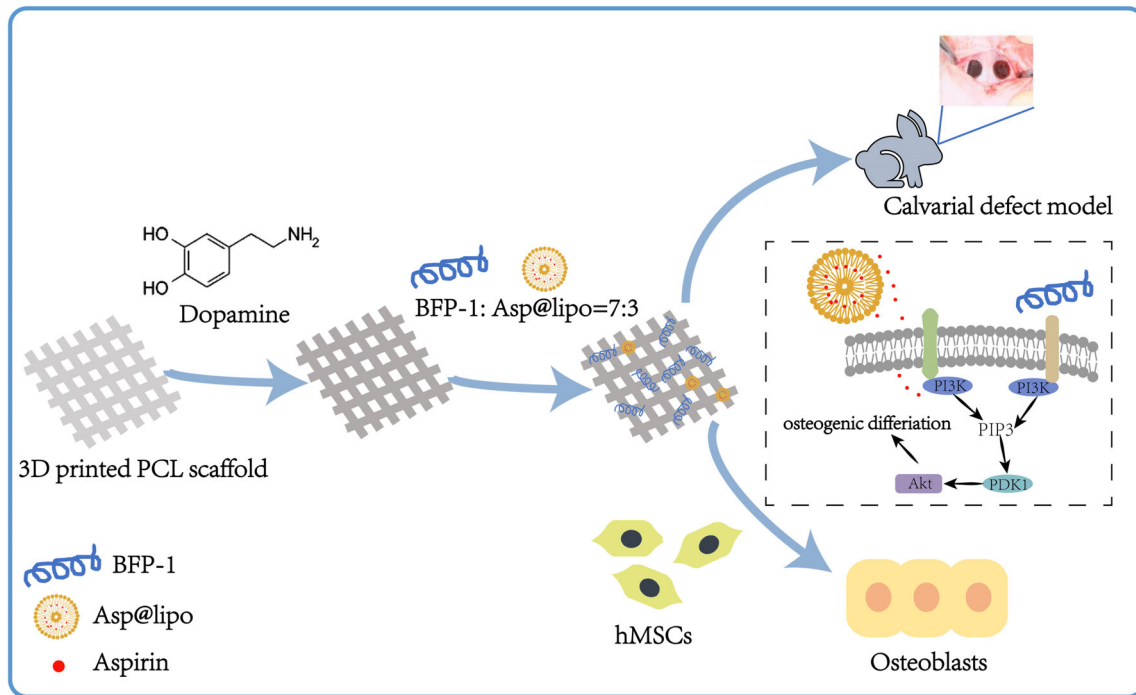


FIGURE 1 Schematic illustration and effects of the composite bioactive scaffold

(DPPC) was obtained from Tokyo Chemical Industry (Tokyo, Japan). All other chemicals were of analytical reagent grade.

2.2 | Immobilization of Asp@Lipo and BFP-1

First, Asp@Lipo was prepared as described previously (He et al., 2014; Li et al., 2019; Liu et al., 2011). Polystyrene (PS) culture plates were decorated with polydopamine (PDA) by pouring dopamine solution (2 mg/ml, pH = 8.5) into the culture plates followed by shaking at 70 rpm and incubation overnight at 37°C. After rinsing twice with phosphate-buffered saline (PBS), the PDA-decorated surface was pretreated with an activation solution (5 mM NHS and 2 mM EDC into 0.1 M MES buffer solution) for 40 min at room temperature. Then the Asp@Lipo (1 mg/ml) and BFP-1 solutions (1 mM) were at various volume ratios (3:7, 5:5, and 7:3, the total volume was 1 ml) added to the PS culture plates and incubated at 4°C for 24 hr. Finally, after washing with PBS, functional substrates were prepared according to the various volume ratios of Asp@Lipo/BFP-1 (3:7, 5:5, and 7:3) and designated as B3A7, B5A5, and B7A3, respectively. Asp@Lipo and BFP-1 were immobilized on the PCL scaffold in the same way. PCL scaffolds were first immersed in the dopamine solution, then treated with an activation solution, and finally decorated with BFP-1 and Asp@Lipo.

2.3 | Characterization of the hybrid surface: Asp@Lipo and BFP-1-decorated PS surface

To verify that the Asp@Lipo and BFP-1 were grafted at the predetermined volume ratios, the bound PE-Rho-loaded Asp@Lipo and

rhodamine-labeled BFP-1 were immobilized on the PS-PDA surfaces and analyzed by confocal laser scanning microscopy (CLSM). The surface morphologies of these functional substrates were also determined by field emission scanning electron microscopy (FE-SEM).

2.4 | Cell culture and proliferation on the hybrid surface

The hMSCs (ScienCell, Carlsbad, CA) were cultured with standard medium consisting of Dulbecco's modified Eagle's medium (DMEM; Hyclone, Logan, UT), fetal bovine serum (FBS, 10%; Gibco, Gaithersburg, MD), penicillin, and streptomycin (1%; Gibco) at 37°C in a 5% CO₂ incubator (Thermo Fisher Scientific, Rockford, IL). The medium was changed every 2 days, and the cell viability at various time points (1 day, 3 days, and 5 day) was evaluated using the Cell Counting Kit-8 assay (CCK-8; Dojindo, Kumamoto, Japan) in accordance with the manufacturer's protocol.

2.5 | Osteogenic differentiation of hMSCs based on different substrates

The hMSCs were seeded onto the hybrid surface, and combined with the predetermined ratios of Asp@Lipo and BFP-1 on two different substrates (PS and PCL). The cells were then cultured with osteogenic induction medium consisting of 0.1 × 10⁻⁶ M dexamethasone (Sigma-Aldrich), 50 µg/ml ascorbic acid (Sigma-Aldrich), and 10 × 10⁻³ M β-glycerol phosphate (Sigma-Aldrich) in standard culture medium. The osteogenic induction medium was changed every other day.

2.6 | Alkaline phosphatase (ALP) and calcium mineralization

To estimate the effects of osteogenic differentiation on the various surfaces decorated with Asp@Lipo and/or BFP-1, staining for the early osteogenic marker ALP, followed by Alizarin red S (ARS) staining for calcium mineralization, was performed on Days 7, 14, and 21. For quantification of ALP activity, the cells were analyzed using an AKP assay kit (NJJ Bio, Nanjing, China) in accordance with the manufacturer's protocol at 7 and 14 days. The total protein concentration was assessed using a bicinchoninic acid protein assay kit (Thermo Fisher) and ALP staining was carried out using an ALP detection kit (CW-BIO, Tianjin, China) according to the manufacturer's instructions. To quantitatively analyze the calcium content, 500 μ l of hexadecylpyridinium chloride (1%; Sigma-Aldrich) was added to each stained sample at 37°C overnight, and the optical density of each sample at 560 nm (OD_{560}) was examined using a microplate reader (Model 680; Bio-Rad, Hercules, CA).

2.7 | Immunofluorescence

After 21 days, following fixation and permeabilization, the hMSCs were incubated with bovine serum albumin buffer (3%) to block non-specific binding. They were then incubated with primary antibodies against osteogenesis-related molecules, that is, human osteopontin (OPN; 1:200 dilution; Abcam, Cambridge, UK) and osteocalcin (OCN; 1:200 dilution; Abcam), at 4°C overnight. After washing with PBS

three times, cells were incubated with secondary antibodies (TRITC-543 goat anti-mouse and FITC-488 goat anti-rabbit [Cell Signaling Technology, Beverly, MA]) at a dilution of 1:500 for 2 hr in the dark. The cells were also stained with 10 μ g/mL DAPI, and fluorescence images were observed immediately by CLSM.

2.8 | Preparation of rabbit calvarial defect model

New Zealand white rabbits (2.0–2.5 kg) were anesthetized by injection of 1% sodium pentobarbital via the auricular vein to prepare the calvarial defect model. All animals were treated in accordance with the guidelines of the Institutional Animal Care and Use Committee of Peking University. For the bone defect model, two defects 8 mm in diameter were prepared in the left and right regions of the calvarial bone, using a trephine (8 mm) to remove bone from the calvarium. The hybrid PCL scaffolds decorated with Asp@Lipo and/or BFP-1 were then transplanted into the calvarial defects thus created, and the animals were observed for 8 weeks. The groups were designated as defect, BFP-1, Asp@Lipo, and B7A3, respectively.

2.9 | Micro-computed tomography (μ CT) and histological assessment

Following euthanasia at 8 weeks after surgery, the cranial bone was harvested and fixed in neutral buffered formalin (10%) for 7 days.

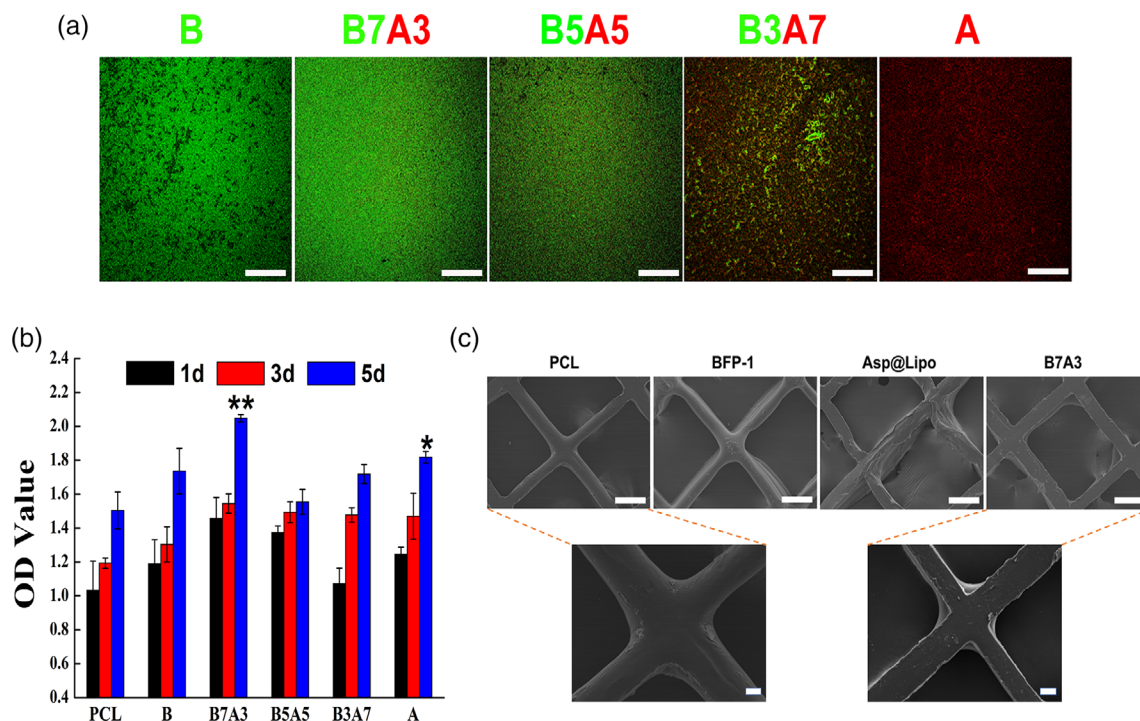


FIGURE 2 Characterization of the culture surface and evaluation of cell compatibility. (a) Characterization of the polystyrene (PS) surface modified by aspirin-based sustained-release system (Asp@Lipo) and bone-forming peptide-1 (BFP-1) (scale bar, 200 μ m). (b) The effects of Asp@Lipo and BFP-1 grafted in different proportions on cell proliferation (* $p < .05$, ** $p < .01$). (c) Characterization of polycaprolactone (PCL) substrates modified by Asp@Lipo and BFP-1 (large scale bars, 100 μ m; small scale bars, 25 μ m)

Then, regenerated bone taken from the defective area was visualized under fixed conditions (60 kV, 0.22 mA, 60 s; 3D reconstructed images) using a μ CT scanner (Inveon MM CT; Siemens AG, Munich, Germany). Meanwhile, trabecular thickness (Tb.Th), trabecular separation (Tb.Sp), trabecular number (Tb.N), and the bone volume fraction (BV/TV) were determined using μ CT. The bone samples were embedded in methylmethacrylate resin and sections were prepared and assessed with toluidine blue staining to quantify bone regeneration.

2.10 | Cell extraction and sequencing analysis

After harvesting the hMSCs from the hybrid PCL scaffolds, total RNA was extracted with TRIzol and their concentrations were measured using a Qubit RNA Assay Kit (Life Technologies, Carlsbad, CA) in accordance with the manufacturer's protocol. Sequencing libraries were prepared with an RNA Library Prep Kit for Illumina (New England Biolabs, Ipswich, MA) in accordance with the manufacturer's protocol. Index-coded sample collection was carried out using a cBot Cluster Generation System in accordance with the manufacturer's instructions (TruSeq PE Cluster Kit v3-cBot-HSkit for Illumina; New England Biolabs). The libraries were then sequenced using the HiSeq platform (Illumina, San Diego, CA)

2.11 | Statistical analysis

All data are presented as the means \pm standard deviation (SD) of at least three representative experiments. Statistical analyses were performed with Origin software and the statistical significance of differences among groups was estimated by Student's *t* test. In all analyses, $p < .05$ was taken to indicate statistical significance.

3 | RESULTS

3.1 | Characterization of the hybrid substrate and evaluation of cell compatibility

Surface decoration and functionalization can be used to control cell behaviors (Yoo, Kim, & Park, 2009). A facile and versatile surface based on dip-coating dopamine solution decoration method for the immobilization of bioactive factors was reported previously (Lee, Dellatore, Miller, & Messersmith, 2007). Dopamine molecules form a pDA structure through self-polymerization under slightly alkaline conditions, which can conjugate with bioactive factors containing amine or thiol moieties through Michael addition (Lee et al., 2007).

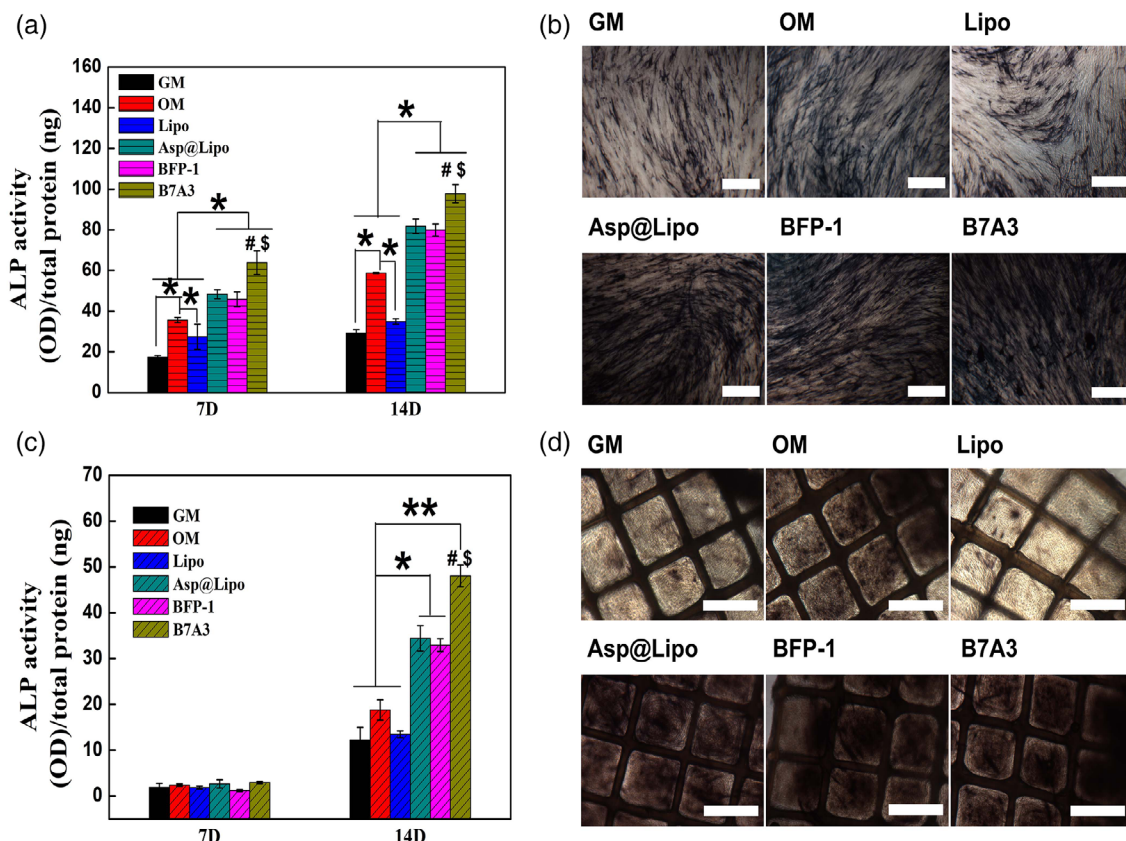


FIGURE 3 Effects on osteogenesis of human mesenchymal stem cells (hMSCs) on different substrates. (a) Alkaline phosphatase (ALP) activity at 7 and 14 days on PS substrates. (b) Representative images of ALP staining on PS substrates. (c) ALP activity at 7 and 14 days on PCL scaffolds. (d) Representative images of ALP staining on PCL scaffolds. # and \$ indicate significant differences between the B7A3 and Asp@Lipo alone and BFP-1 alone groups, respectively (#, \$, and *, $p < .05$; **, $p < .01$). Results are representative of at least three independent experiments. Scale bars, 200 μ m

Covalently grafted bioactive factors are not easily eliminated from decorated substrates on long-term application, so are promising for use in tissue engineering (Das & Zouani, 2014).

PE-Rho liposomes and FITC-BFP-1 were used to verify whether the bioactive molecules were successfully grafted onto the substrate. Figure 2 shows representative fluorescence signals of various decorated surfaces; both Asp@Lipo and BFP-1 were successfully grafted onto the substrates. In addition, the green fluorescence intensity decreased, while the red fluorescence intensity increased markedly, with decreasing grafted FITC-BFP-1 to PE-Rho liposome (B7A3, B5A5, B3A7) concentration ratio (Figure S1).

To regulate the differentiation of stem cells, it is necessary to consider the proliferation of cells, and their adhesion to the substrate, which are both important factors (Das & Zouani, 2014). After verifying that the Asp@Lipo and BFP-1 could be successfully grafted onto the PS substrate, we also grafted the two bioactive factors onto another substrate (PCL scaffold) to investigate the adherence and proliferation of hMSCs. As shown in Figure 2, cell proliferation in all samples was time-dependent, indicating no cytotoxicity in the tested samples. Furthermore, the hMSCs grew rapidly on the B7A3-based substrate and

the OD₄₅₀ was highest in all groups at Day 5. We also investigated alterations in the surface morphology of these functional substrates by SEM. As shown in Figure 2, compared to the pure smooth PCL scaffold, the BFP-1 and/or Asp@Lipo-decorated PCL composite scaffold was rougher, with more bioactive factors at the intersections of composite scaffolds. Thus, the hybrid substrate containing Asp@Lipo and BFP-1 played an active role in the adhesion and proliferation of stem cells.

3.2 | In vitro osteogenic differentiation of hMSCs on hybrid substrate

To study the osteogenic differentiation of hMSCs on hybrid Asp@Lipo and/or BFP-1-based substrates (PS and PCL scaffolds), we investigated the expression of ALP, a phosphate and calcium binding protein, which is expressed strongly in osteoblasts (Zheng et al., 2014). As shown in Figure 3, the hMSCs were seeded on two different substrates (PS and PCL) and cultured for 2 weeks. The control groups were GM (hMSCs cultured in general media without osteogenic factors; negative control) and OM (hMSCs cultured in osteogenic media;

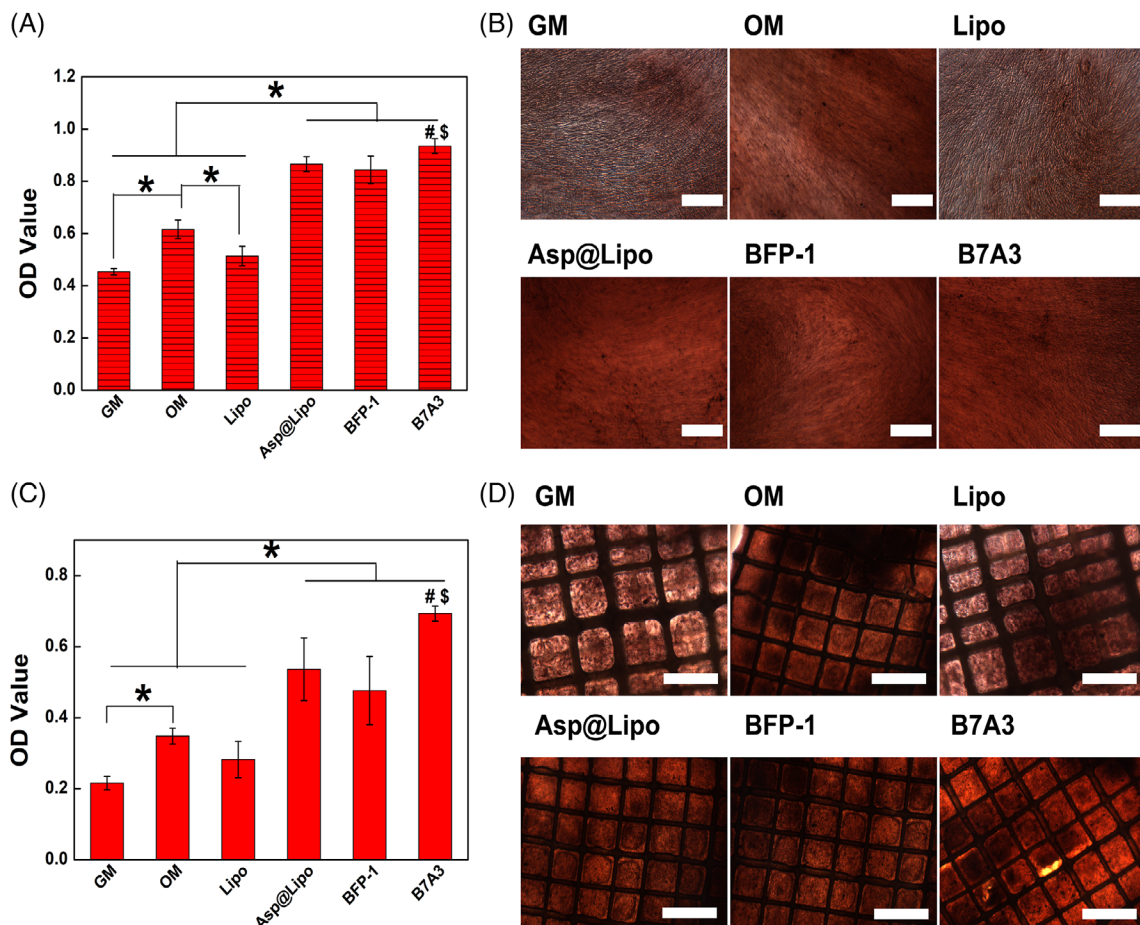


FIGURE 4 Calcium deposition of hMSCs on different substrates. (a) Calcium deposition at 7 and 14 days on PS substrates. (b) Representative image of ARS staining on PS substrates. (c) Calcium deposition at 7 and 14 days on PCL scaffolds. (d) Representative image of Alizarin red S (ARS) staining on PCL scaffolds. # and \$ indicate significant differences between B7A3 and the Asp@Lipo alone and BFP-1 alone groups, respectively (#, \$, and *, $p < .05$). Results are representative of at least three independent experiments. Scale bars, 400 μ m

positive control). The ALP activity of hMSCs in the Asp@Lipo plus BFP-1 group was higher than those in the GM, OM, and Asp@Lipo alone groups at day 14 (Figure 3). In addition, the level of ALP expression by hMSCs in the B7A3 group was markedly upregulated, showing the highest level among all groups. The B7A3 group showed a significant difference in ALP activity compared to the control groups ($p < .01$), indicating an advantage over the Asp@Lipo alone and BFP-1 alone groups ($p < .05$). Thus, the B7A3-based hybrid substrate facilitated osteogenic differentiation of hMSCs and has potential for application in tissue engineering.

To further validate the results of osteogenesis activity (ALP) on the hybrid substrate, calcium deposition was assessed by ARS staining. Immunofluorescence staining was also performed to detect

the expression of the osteogenesis-related proteins, OCN and OPN, in the later stage of osteogenesis. Consistent with the ALP results, hMSCs in the B7A3 group showed more obvious bone-like nodules and calcium deposition compared to the other groups at 21 days (Figure 4); the results of immunofluorescence staining were similar. As shown in Figure 5, noticeable improvements in signaling of osteogenesis-related proteins was seen on CLSM, due to the surface decoration of Asp@Lipo and BFP-1 on the substrate.

Taken together, these observations indicated that bioactive factors, such as Asp@Lipo and BFP-1, could be successfully immobilized on the substrates, regardless of the use of ordinary PS culture plates or PCL scaffold. More importantly, a ratio of Asp@Lipo/BFP-1 of 3:7 (i.e., B7A3 scaffold) yielded the greatest improvement in osteogenic

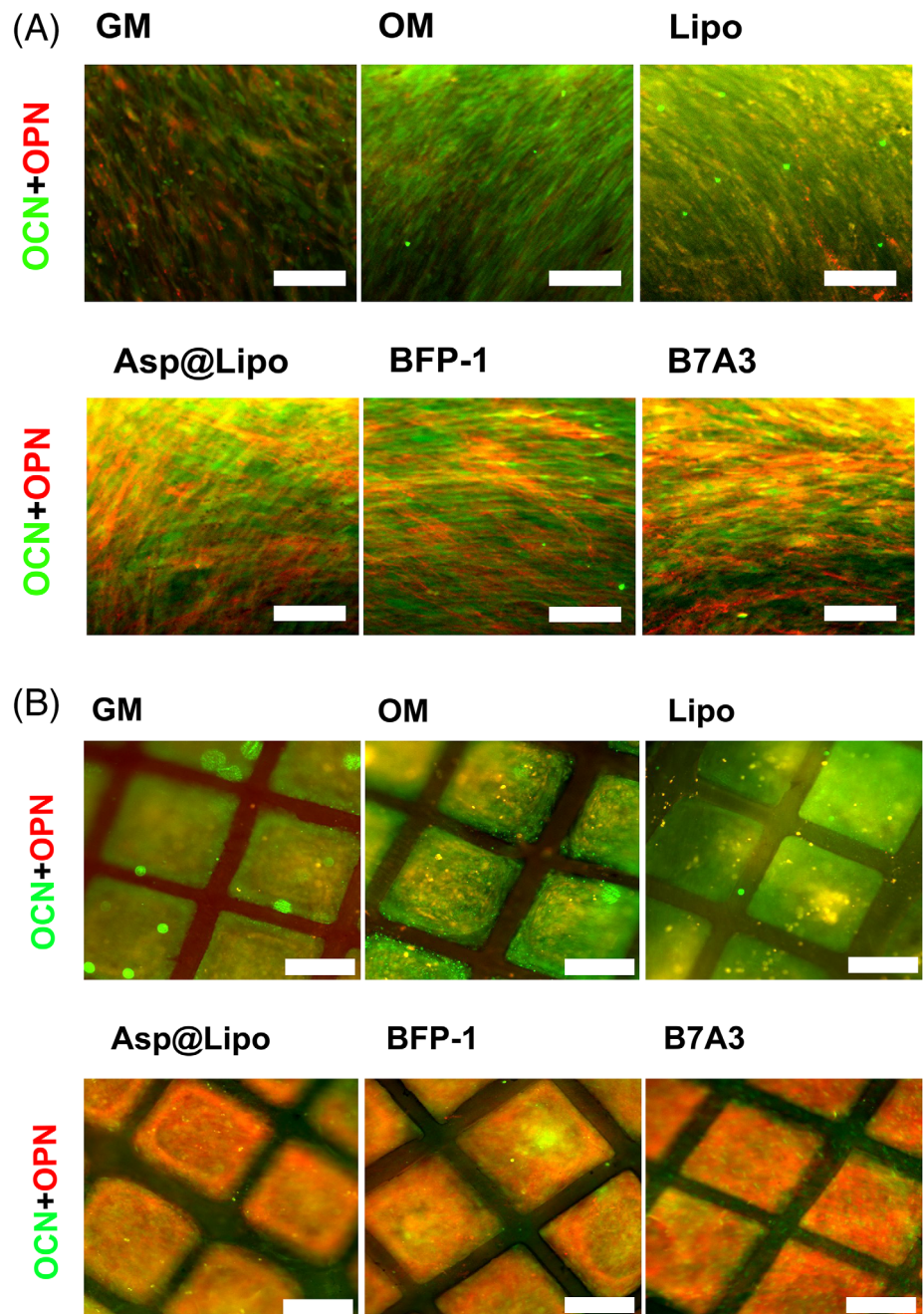


FIGURE 5 Representative immunofluorescence images show the distributions of osteocalcin (OCN; green) and osteopontin (OPN; red) on PS (a) and PCL (b) substrates at Day 21. Scale bars, 100 μ m

differentiation efficiency of hMSCs; this result could accelerate the application of hMSCs in bone tissue engineering.

3.3 | In vivo bone regeneration in calvarial defect model

The in vivo bone regeneration of the hybrid scaffolds was estimated at 8 weeks after the surgery. As seen in the 3D reconstructed micro-CT images (Figure 6), compared to the defect group (control group, $17.56 \pm 5.58\%$ bone volume), which showed only limited bone formation at the defect edges, significant enhancement of new bone tissue infiltration at the bone cavity was detected in the groups treated with the hybrid substrates, that is, BFP-1 ($28.84 \pm 4.18\%$ bone volume), Asp@Lipo ($35.65 \pm 3.65\%$ bone volume), and B7A3 ($45.12 \pm 2.75\%$ bone volume). The group treated with B7A3 hybrid scaffold showed more obvious bone tissue formation, which extended into the center of the bone cavity, than the defect control group ($p < .01$), thus indicating its powerful osteoinductive effect and outstanding bone regeneration ability. Indices of bone histomorphometry were also examined. Tb.Th and Tb.N showed significant improvement in the B7A3 group compared to the defect-only group. The B7A3 group

showed superior reduction of Tb.Sp compared to the other three groups, indicating the favorable contribution of our B7A3 hybrid scaffold to bone regeneration.

To characterize the regenerated bone in more detail, the implant samples were subjected to immunohistochemical staining, which provided further evidence of the contribution of our B7A3 hybrid scaffold to bone regeneration. Significantly greater bone integration into the B7A3 scaffold surface was detected compared to the other three groups (Figure 7). The defect-only group showed little newly formed bone. The results of in vivo experiments showed that the application of our B7A3 hybrid scaffold played an active role in bone regeneration, consistent with the conclusions based on in vitro experiments. The B7A3 hybrid scaffold showed excellent ability to support osteogenesis, and should therefore be useful in bone tissue engineering.

3.4 | Analysis of differentially expressed genes

First, we performed gene clustering analysis between different samples. As shown in Figure S2, there were differences in gene expression among the groups. To determine the overall distribution of the

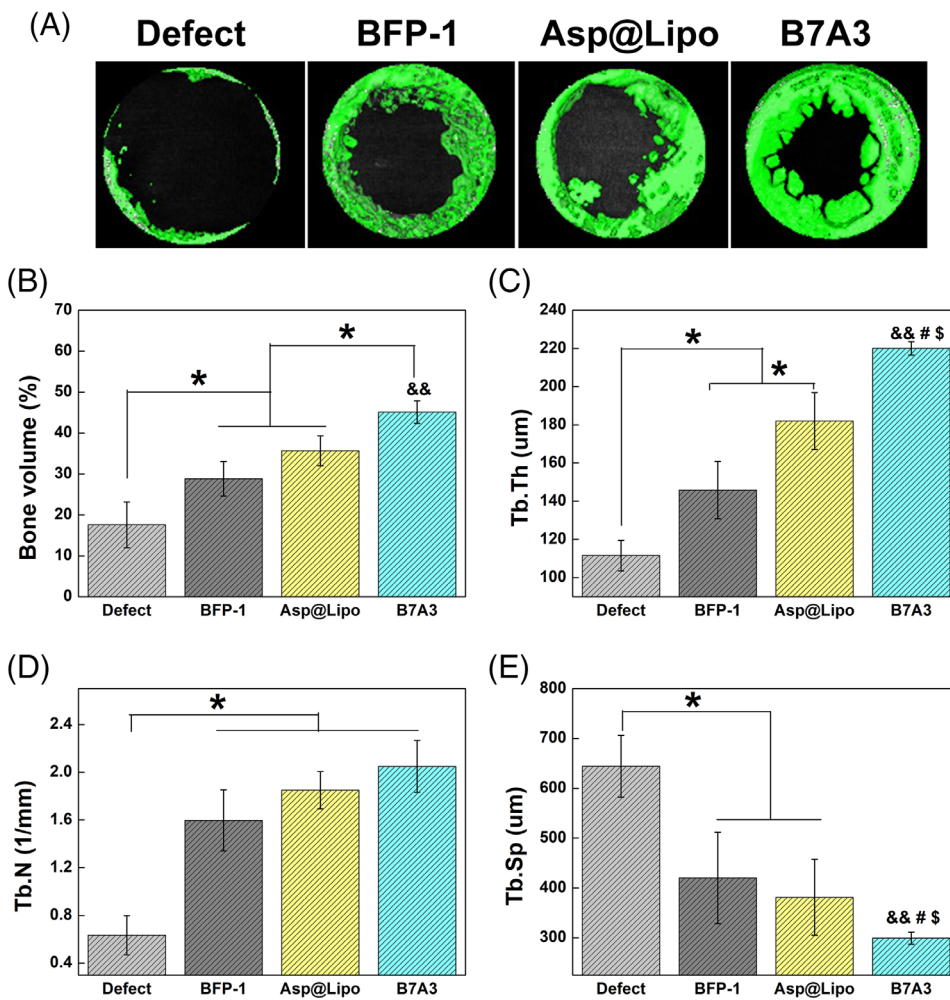


FIGURE 6 The 3D reconstructed micro-CT images of mineralization and quantitative bone histomorphological indexes. (a) Micro-computed tomography (μCT) images. (b) Bone volume (BV). (c) Trabecular thickness (Tb.th). (d) Trabecular number (Tb.N). (e) Trabecular separation (Tb.Sp)

differentially expressed genes (DEGs), we used the volcano plot with the threshold set as $|\log_2(\text{fold change})| > 1$ and $q < .005$. Then, we screened the DEGs; as shown in Figure 8, compared to the control groups (GM and OM), and to BFP-1 alone and Asp@Lipo alone, B7A3

group showed significant differences in the upregulation and downregulation of various genes.

Furthermore, to determine the numbers of common and unique DEGs between different samples, we compared the list of DEGs obtained for each group using a Venn diagram (Figure S3); the sum of the numbers in the circles represents the total number of DEGs among all samples. As shown in Figure S2, there were 629, 163, 228, and 225 DEGs between the B7A3 and GM, OM, BFP, and Asp@Lipo groups, respectively.

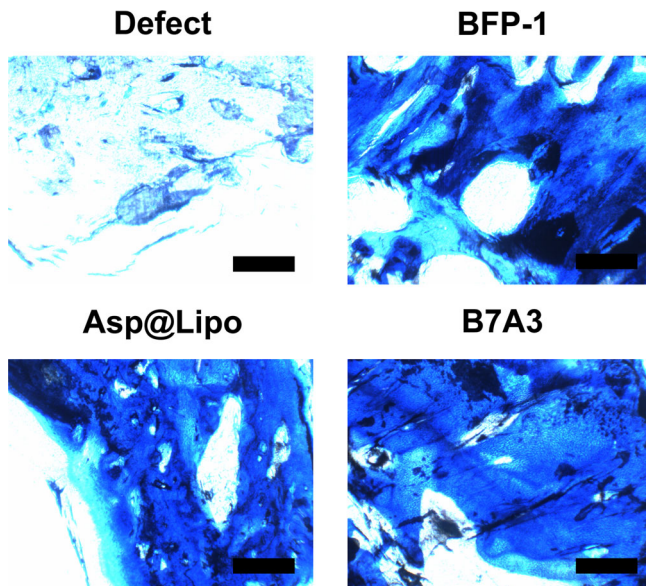


FIGURE 7 Toluidine blue staining. Scale bars, 100 μm

3.5 | Gene ontology (GO) analysis

To categorize the DEGs by function, we performed GO enrichment analysis. The GO classification system is mainly composed of biological processes, cell components, and molecular functions. As shown in the histogram in Figure 9, with regard to biological processes, the DEGs were mainly related to the maintenance of basic activities and functions of cells, such as localization and growth, protein secretion, immune response, and angiogenesis. The DEGs were mainly concentrated in the extracellular protein matrix and collagen polymer and, in the molecular functional terms, were mainly related to the activity of transferases, chemokines, growth factors, and proteins, as well as calcium ion transport and binding, and ion channels. Based on the above results, we posited that most of the DEGs

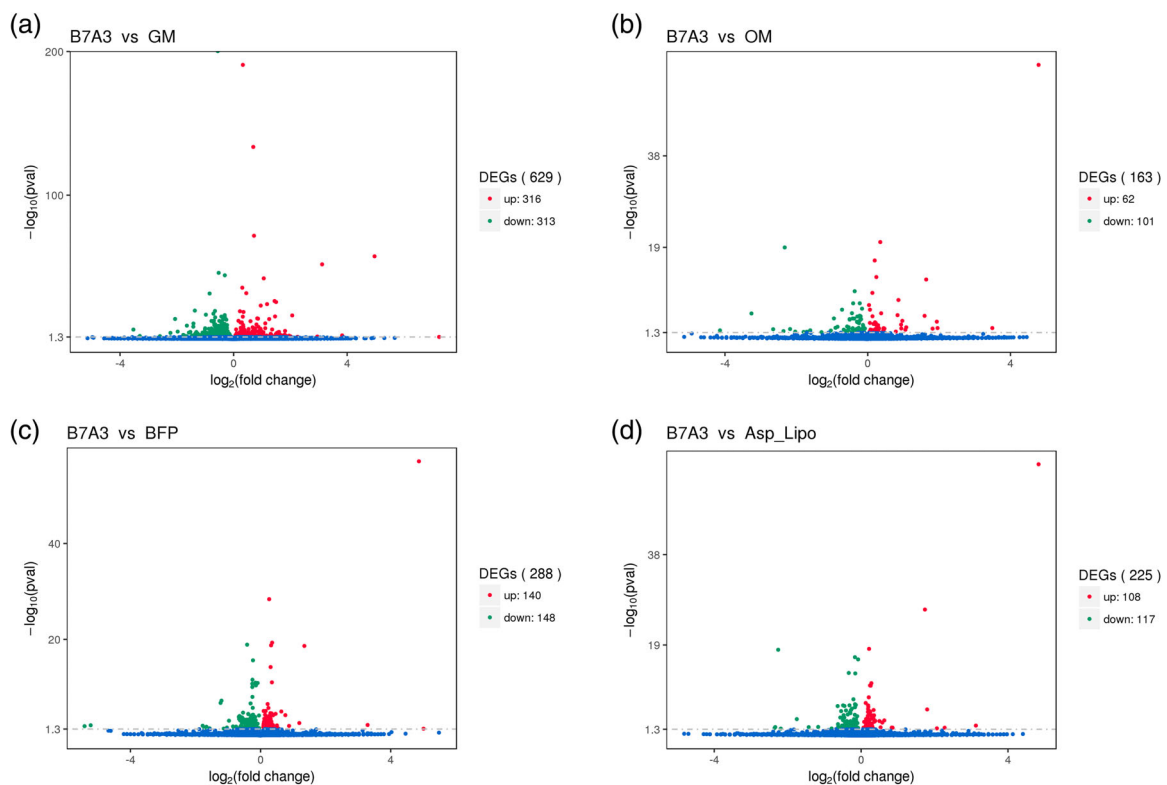


FIGURE 8 Volcano plot (red dots are significantly upregulated genes and green dots are significantly downregulated genes)

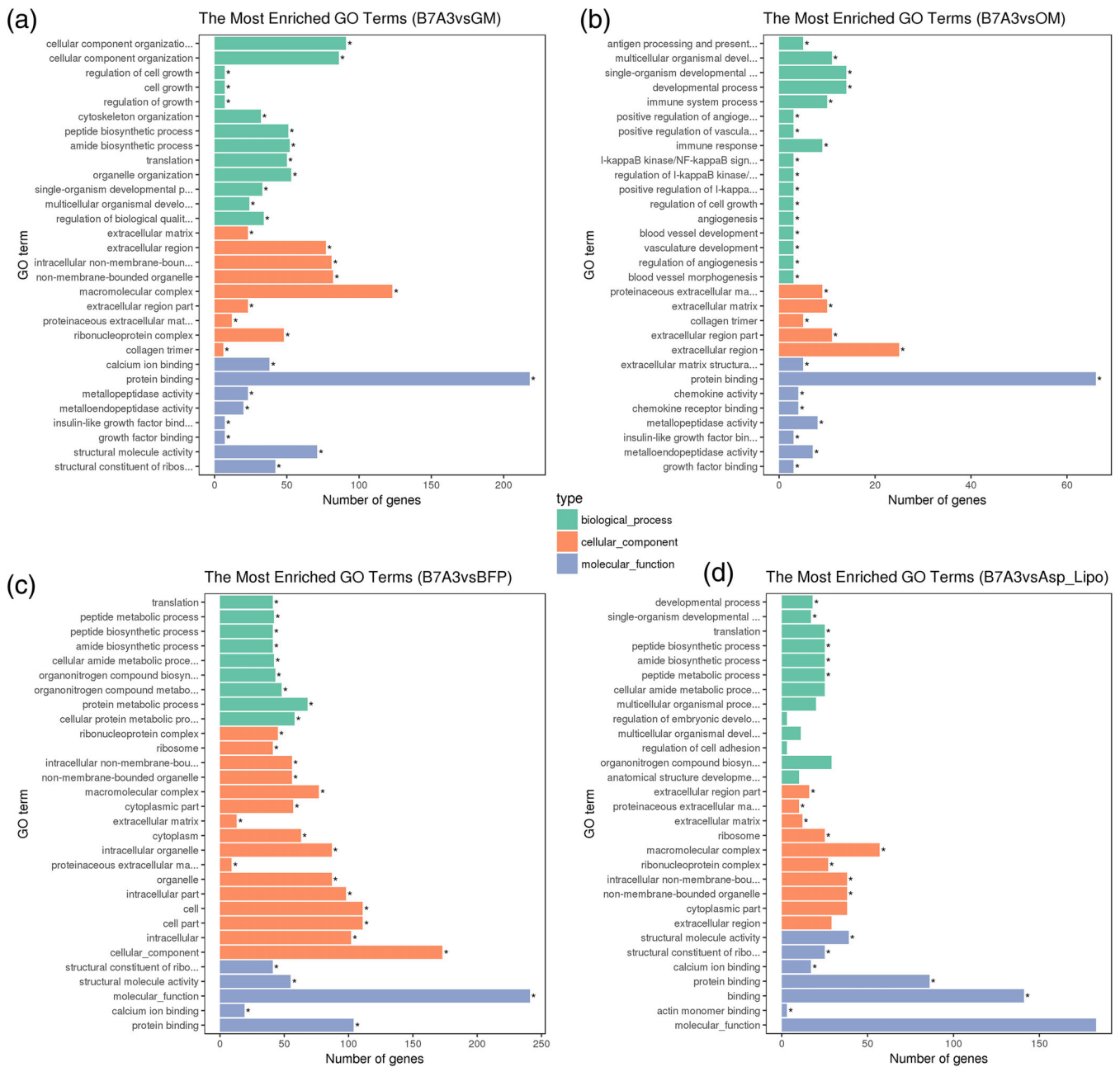


FIGURE 9 Histogram of Gene Ontology (GO) enrichment terms of differentially expressed genes

were cytokines involved in fundamental biological processes or osteogenesis.

3.6 | Kyoto Encyclopedia of genes (KEGG) analysis

To clarify the effects of in vitro culture of stem cells on signaling pathways involved in bone differentiation, we used the KEGG database to determine differences in gene expression based on q values. Compared to the GM, OM, BFP alone, and Asp@Lipo groups, the DEGs in the B7A3 group were mainly enriched in the PI3K-Akt signaling pathway; significant differences in cell adhesion molecules, adhesion

plaques, ribosomes, phagosomes, cytoskeleton, and extracellular matrix were observed (Figure 10).

4 | DISCUSSION

Currently, the treatment methods for bone defects are not perfect. There are still some problems such as secondary injury, poor shaping, and immune rejection in autogenous and allogeneic bone transplantation. Distraction osteogenesis technology is difficult to popularize due to its high price, complex operation technology, limited indications. As a result, bone tissue engineering may be one of the most effective

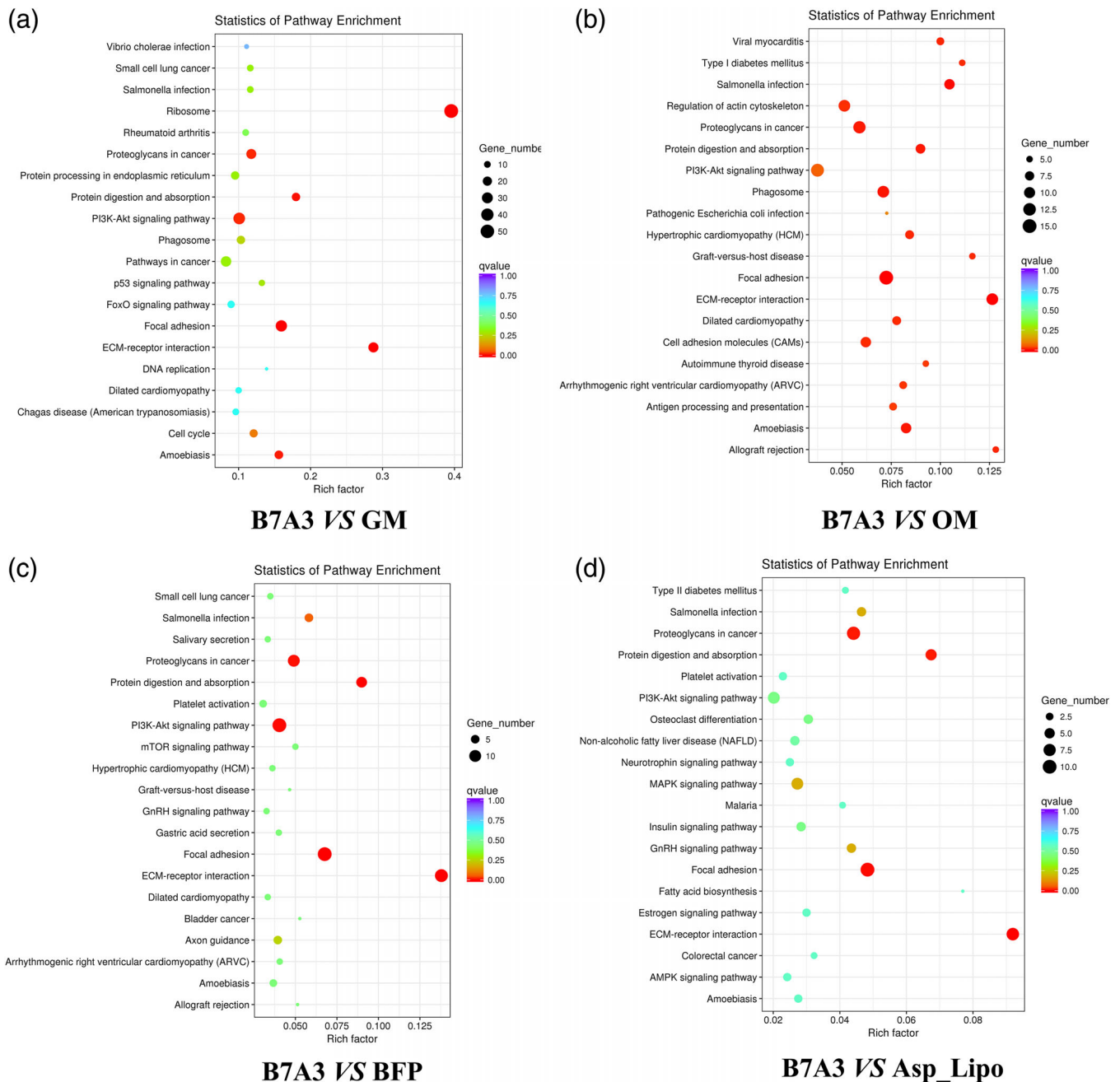


FIGURE 10 Kyoto Encyclopedia of Genes (KEGG) analysis

methods for the treatment of bone defects in the future. In this study, we prepared a composite bioactive scaffold (PCL-Asp@Lipo) for bone tissue engineering. The surface of the 3D-printed PCL scaffold was functionalized with the Asp@Lipo and BFP-1, which could achieve sustained release.

Immunofluorescence images showed that Asp@Lipo and BFP-1 were successfully grafted onto PS plate by means of dip-coating dopamine solution decoration. Then Asp@Lipo and BFP-1 were grafted onto PCL scaffold in different proportions. When the graft ratio of Asp@Lipo to BFP-1 was 3:7, it was beneficial to the adhesion and proliferation of hMSC, which indicated that the decorated scaffold was cellularly compatible. SEM images showed that the rough

scaffold surface which was decorated with Asp@Lipo and BFP-1. Furthermore, the ALP activity of PCL scaffold was modified with Asp@Lipo and BFP-1 at ratio of 3:7 increased significantly. Through ARS staining, hMSCs showed more obvious calcium nodules and calcium deposition on the modified scaffold. In addition, Immunofluorescence showed the expression of OCN and OPN. These results fully indicated that Asp@Lipo and BFP-1 can play a synergistic role, and further enhance the osteogenic differentiation efficiency of hMSCs to a greater extent.

To further verify the osteogenic ability of the scaffold, modified PCL scaffold was transplanted into the calvarial defect. Eight weeks after surgery, the results of micro-CT 3D reconstruction showed that

compared with the defect group, the bone volume of BFP-1 group, Asp@Lipo group and B7A3 group increased by 64.2, 103.0, and 156.9%, respectively. This suggests that decorated scaffold can significantly enhance new bone formation at the defect site. Among them, the B7A3 composite scaffold implantation can cause more new bone formation and more obvious expansion to the bone cavity center. Quantitative measurement also showed compared with defect group, Tb.Th and Tb.N of dual factor composite scaffold increased by 2 times and 2.3 times, respectively, while Tb.Sp decreased to 46.2%. Furthermore, the results of toluidine blue staining indicated that the bone regeneration ability of the PCL-B7A3 composite bioactive scaffold was significantly improved compared to the PCL-Asp@Lipo alone and PCL-BFP-1 alone scaffolds. The in vivo implantation of bioactive composite PCL scaffolds can promote the role of bone repair. These results sufficiently indicated that Aspirin and BFP-1 could exert synergistic effect to stimulate the bone induction process and promote the formation of new bone. The dual-factor composite PCL scaffold has better and stronger bone regeneration ability, which could be application in bone tissue engineering and regenerative medicine fields.

As osteogenesis potential is based on a complex gene regulatory network, we analyzed the functions of DEGs through transcriptome sequencing analysis of composite and noncomposite scaffolds, without any modification of the hMSC transcriptome. Furthermore, GO and KEGG analyses were performed and showed that the bone remodeling-promoting effect of the composite scaffold was mainly related to the PI3K/Akt signal pathway. The PI3K/Akt signaling pathway is involved in physiological activities, such as the regulation of cell proliferation, adhesion, differentiation, apoptosis, and metabolism (Isomoto et al., 2007). Phosphatidylinositol 3-kinase (PI3K), a member of the lipid kinase family, is located upstream of the serine/threonine kinase Akt. It can first regulate cell proliferation and metabolism by phosphorylating the Ser473 residues of its downstream AKT carbon terminal, thereby further activating AKT, T cell, B cell, G protein-coupled and cytokine receptors, integrin, and receptor tyrosine kinase signaling (Ge et al., 2018). Moreover, the PI3K/Akt signaling pathway has a significant regulatory role in the formation and differentiation of osteoblasts and osteoclasts (Harada & Rodan, 2003; Jin et al., 2017; Wu, Guo, Yang, & Ni, 2017). Many studies have demonstrated a close relationship between the PI3K/Akt signaling pathway and bone tissue metabolism. For example, icariin was shown to regulate the PI3K/Akt signaling pathway, and to have a preventive effect against osteoporosis caused by glucocorticoid treatment (Hu et al., 2017). Salvianic acid can also activate the PI3K/Akt signaling pathway, reducing osteoporosis in a rat model of osteoblast apoptosis. Similar to previous reports, our results showed that the composite B7A3 scaffold promoted bone regeneration mainly through the PI3K/Akt signaling pathway. Therefore, the PI3K/Akt signaling pathway is closely related to the metabolism of bone tissue, and a detailed understanding and in-depth study of the characteristics of this pathway will be beneficial for furthering the development of bone tissue engineering.

These results suggest that the 3D-printed PCL scaffold decorated Asp@Lipo and BFP-1 at a ratio of 3:7 has significant osteogenic ability, which not only can promote osteogenic differentiation of hMSCs,

but also can repair bone defects. The aspirin and BFP-1 can stimulate the bone induction process and promote the formation of new bone in synergistic way.

5 | CONCLUSIONS

In this study, we successfully integrated aspirin liposomes (Asp@Lipo) and BFP-1 at a ratio of 3:7 onto 3D-printed PCL scaffold. A series of in vitro osteoblastic experiments and a rabbit cranial defect model showed that the aspirin and BFP-1 of the composite scaffolds not only can stimulate osteogenic differentiation of hMSCs, but also can promote the formation of new bone in synergistic way. Furthermore, GO and KEGG analyses showed that the bone remodeling-promoting effect of the composite scaffold was mainly related to the PI3K/Akt signal pathway. As a safe and efficient composite material, the dual-factor composite scaffold is expected to be better applied in the field of bone tissue engineering and regenerative medicine. This may also help to further develop the composite bone biomaterials with immune effects, and promote development of bone tissue engineering.

CONFLICT OF INTEREST

The authors declare no conflict of interest.

REFERENCES

- Anselmo, A. C., & Mitragotri, S. (2014). An overview of clinical and commercial impact of drug delivery systems. *Journal of Controlled Release*, 190, 15–28.
- Arbolea, L., & Castañeda, S. (2013). Osteoimmunology: The study of the relationship between the immune system and bone tissue. *Reumatología Clínica*, 9(5), 303–315.
- Arron, J. R., & Choi, Y. (2000). Osteoimmunology—Bone versus immune system. *Nature*, 408(6812), 535–536.
- Bajpai, A. K., Shukla, S. K., Bhanu, S., & Kankane, S. (2008). Responsive polymers in controlled drug delivery. *Progress in Polymer Science*, 33(11), 1088–1118.
- Bawa, P., Pillay, V., Choonara, Y. E., & du Toit, L. C. (2009). Stimuli-responsive polymers and their applications in drug delivery. *Biomedical Materials*, 4(2), 022001.
- Beederman, M., Lamplot, J. D., Nan, G., Wang, J., Liu, X., Yin, L., et al. (2013). BMP signaling in mesenchymal stem cell differentiation and bone formation. *Journal of Biomedical Science and Engineering*, 6(8A), 32–52.
- Bessa, P. C., Machado, R., Nurnberger, S., Dopler, D., Banerjee, A., Cunha, A. M., et al. (2010). Thermoresponsive self-assembled elastin-based nanoparticles for delivery of BMPs. *Journal of Controlled Release*, 142(3), 312–318.
- Carson, J. S., & Bostrom, M. P. (2007). Synthetic bone scaffolds and fracture repair. *Injury*, 38(Suppl 1), S33–S37.
- Cook, E. A., & Cook, J. J. (2009). Bone graft substitutes and allografts for reconstruction of the foot and ankle. *Clinics in Podiatric Medicine and Surgery*, 26(4), 589–605.
- Das, R. K., & Zouani, O. F. (2014). A review of the effects of the cell environment physicochemical nanoarchitecture on stem cell commitment. *Biomaterials*, 35(20), 5278–5293.
- Dimitriou, R., Tsiridis, E., & Giannoudis, P. V. (2005). Current concepts of molecular aspects of bone healing. *Injury*, 36(12), 1392–1404.
- Fernandez-Tresguerres-Hernandez-Gil, I., Alobera-Gracia, M. A., del-Canto-Pingarron, M., & Blanco-Jerez, L. (2006). Physiological bases of

- bone regeneration II. The remodeling process. *Medicina Oral, Patologia Oral Y Cirugia Bucal*, 11(2), E151–E157.
- Fernandez-Tresguerres-Hernandez-Gil, I., Alobera-Gracia, M. A., del-Canto-Pingarron, M., & Blanco-Jerez, L. (2006). Physiological bases of bone regeneration I. histology and physiology of bone tissue. *Medicina Oral, Patologia Oral Y Cirugia Bucal*, 11(1), E47–E51.
- Ge, Y., Liu, H., Qiu, X., Ma, G., Wang, H., Du, M., et al. (2018). Genetic variants in PI3K/Akt/mTOR pathway genes contribute to gastric cancer risk. *Gene*, 670, 130–135.
- Harada, S., & Rodan, G. A. (2003). Control of osteoblast function and regulation of bone mass. *Nature*, 423(6937), 349–355.
- He, S., Zhou, P., Wang, L., Xiong, X., Zhang, Y., Deng, Y., & Wei, S. (2014). Antibiotic-decorated titanium with enhanced antibacterial activity through adhesive polydopamine for dental/bone implant. *Journal of the Royal Society Interface*, 11(95), 20140169.
- Hu, J., Mao, Z., He, S., Zhan, Y., Ning, R., Liu, W., ... Yang, J. (2017). Icarin protects against glucocorticoid induced osteoporosis, increases the expression of the bone enhancer DEC1 and modulates the PI3K/Akt/GSK3beta/beta-catenin integrated signaling pathway. *Biochemical Pharmacology*, 136, 109–121.
- Isomoto, S., Hattori, K., Ohgushi, H., Nakajima, H., Tanaka, Y., & Takakura, Y. (2007). Rapamycin as an inhibitor of osteogenic differentiation in bone marrow-derived mesenchymal stem cells. *Journal of Orthopaedic Science*, 12(1), 83–88.
- Jain KK. 2008. Drug delivery systems—An overview. *Drug Delivery Systems*. pp. 1–50.
- Jin, X., Sun, J., Yu, B., Wang, Y., Sun, W. J., Yang, J., ... Xie, W. L. (2017). Daidzein stimulates osteogenesis facilitating proliferation, differentiation, and antiapoptosis in human osteoblast-like MG-63 cells via estrogen receptor-dependent MEK/ERK and PI3K/Akt activation. *Nutrition Research*, 42, 20–30.
- Kawaguchi, H., Kurokawa, T., Hanada, K., Hiyama, Y., Tamura, M., Ogata, E., & Matsumoto, T. (1994). Stimulation of fracture repair by recombinant human basic fibroblast growth-factor in normal and streptozotocin-diabetic rats. *Endocrinology*, 135(2), 774–781.
- Kim, H. K., Kim, J. H., Park, D. S., Park, K. S., Kang, S. S., Lee, J. S., ... Yoon, T. R. (2012). Osteogenesis induced by a bone forming peptide from the prodomain region of BMP-7. *Biomaterials*, 33(29), 7057–7063.
- Lee, H., Dellatore, S. M., Miller, W. M., & Messersmith, P. B. (2007). Mussel-inspired surface chemistry for multifunctional coatings. *Science*, 318(5849), 426–430.
- Li, Y., Bai, Y., Pan, J., Wang, H., Li, H., Xu, X., et al. (2019). A hybrid 3D-printed aspirin-laden liposome composite scaffold for bone tissue engineering. *Journal of Materials Chemistry B*, 7(4), 619–629.
- Lind, M., & Bunger, C. (2001). Factors stimulating bone formation. *European Spine Journal*, 10(Suppl 2), S102–S109.
- Liu, Y., Wang, L., Kikuri, T., Akiyama, K., Chen, C., Xu, X., ... Shi, S. (2011). Mesenchymal stem cell-based tissue regeneration is governed by recipient T lymphocytes via IFN-gamma and TNF-alpha. *Nature Medicine*, 17(12), 1594–1601.
- Oliveira, R., Hage, M. E., Carrel, J. P., Lombardi, T., & Bernard, J. P. (2012). Rehabilitation of the edentulous posterior maxilla after sinus floor elevation using deproteinized bovine bone: A 9-year clinical study. *Implant Dentistry*, 21(5), 422–426.
- Oryan, A., Alidadi, S., Moshiri, A., & Bigham-Sadegh, A. (2014). Bone morphogenetic proteins: A powerful osteoinductive compound with non-negligible side effects and limitations. *BioFactors*, 40(5), 459–481.
- Perets, A., Baruch, Y., Weisbuch, F., Shoshany, G., Neufeld, G., & Cohen, S. (2003). Enhancing the vascularization of three-dimensional porous alginate scaffolds by incorporating controlled release basic fibroblast growth factor microspheres. *Journal of Biomedical Materials Research Part A*, 65A(4), 489–497.
- Sambuceti, G., Morbelli, S., Vanella, L., Kusmic, C., Marini, C., Massollo, M., et al. (2009). Diabetes impairs the vascular recruitment of normal stem cells by oxidant damage, reversed by increases in pAMPK, heme oxygenase-1, and adiponectin. *Stem Cells*, 27(2), 399–407.
- Saran, U., Gemini Piperni, S., & Chatterjee, S. (2014). Role of angiogenesis in bone repair. *Archives of Biochemistry and Biophysics*, 561, 109–117.
- Schindler, O. S., Cannon, S. R., Briggs, T. W., & Blunn, G. W. (2007). Use of a novel bone graft substitute in peri-articular bone tumours of the knee. *The Knee*, 14(6), 458–464.
- Schmitz, J. P., & Hollinger, J. O. (1986). The critical size defect as an experimental-model for craniomandibulofacial nonunions. *Clinical Orthopaedics and Related Research*, 205, 299–308.
- Smilek, D. E., Ehlers, M. R., & Nepom, G. T. (2014). Restoring the balance: Immunotherapeutic combinations for autoimmune disease. *Disease Models & Mechanisms*, 7(5), 503–513.
- Staiger, M. P., Pietak, A. M., Huadmai, J., & Dias, G. (2006). Magnesium and its alloys as orthopedic biomaterials: A review. *Biomaterials*, 27(9), 1728–1734.
- Takayanagi, H. (2007). Osteoimmunology: Shared mechanisms and crosstalk between the immune and bone systems. *Nature Reviews. Immunology*, 7(4), 292–304.
- Trueta, J. (1963). The role of the vessels in osteogenesis. *Journal of Bone and Joint Surgery-British*, 45(2), 402–418.
- Tsiridis, E., Upadhyay, N., & Giannoudis, P. (2007). Molecular aspects of fracture healing: Which are the important molecules? *Injury*, 38(Suppl 1), S11–S25.
- Vo, T. N., Kasper, F. K., & Mikos, A. G. (2012). Strategies for controlled delivery of growth factors and cells for bone regeneration. *Advanced Drug Delivery Reviews*, 64(12), 1292–1309.
- Wang, J., Tang, J., Zhang, P., Li, Y., Wang, J., Lai, Y., & Qin, L. (2012). Surface modification of magnesium alloys developed for bioabsorbable orthopedic implants: A general review. *Journal of Biomedical Materials Research. Part B, Applied Biomaterials*, 100(6), 1691–1701.
- Wu, L., Guo, Q., Yang, J., & Ni, B. (2017). Tumor necrosis factor alpha promotes osteoclast formation via PI3K/Akt pathway-mediated Blimp1 expression upregulation. *Journal of Cellular Biochemistry*, 118(6), 1308–1315.
- Yoo, H. S., Kim, T. G., & Park, T. G. (2009). Surface-functionalized electrospun nanofibers for tissue engineering and drug delivery. *Advanced Drug Delivery Reviews*, 61(12), 1033–1042.
- Zadpoor, A. A., & Malda, J. (2017). Additive manufacturing of biomaterials, tissues, and organs. *Annals of Biomedical Engineering*, 45(1), 1–11.
- Zheng, C., Wang, J., Liu, Y., Yu, Q., Liu, Y., Deng, N., & Liu, J. (2014). Functional selenium nanoparticles enhanced stem cell osteoblastic differentiation through BMP signaling pathways. *Advanced Functional Materials*, 24(43), 6872–6883.

SUPPORTING INFORMATION

Additional supporting information may be found online in the Supporting Information section at the end of this article.

How to cite this article: Li Y, Li Q, Li H, et al. An effective dual-factor modified 3D-printed PCL scaffold for bone defect repair. *J Biomed Mater Res*. 2020;1–13. <https://doi.org/10.1002/jbm.b.34555>